

REVISITING THE SCALING RELATIONS OF BLACK HOLE MASSES AND HOST GALAXY PROPERTIES

NICHOLAS J. MCCONNELL^{1,2} AND CHUNG-PEI MA²

Draft version December 3, 2024

ABSTRACT

New kinematic data and modeling efforts in the past few years have substantially expanded and revised dynamical measurements of black hole masses (M_{\bullet}) at the centers of nearby galaxies. Here we compile an updated sample of 72 black holes and their host galaxies, and present revised scaling relations between M_{\bullet} and stellar velocity dispersion (σ), V-band luminosity (L), and bulge stellar mass (M_{bulge}), for different galaxy subsamples. Our best-fitting power law relations for the full galaxy sample are $\log_{10}(M_{\bullet}) = 8.33 + 5.57 \log_{10}(\sigma/200 \text{ km s}^{-1})$, $\log_{10}(M_{\bullet}) = 9.23 + 1.11 \log_{10}(L/10^{11} L_{\odot})$, and $\log_{10}(M_{\bullet}) = 8.46 + 1.05 \log_{10}(M_{\text{bulge}}/10^{11} M_{\odot})$. A log-quadratic fit to the $M_{\bullet} - \sigma$ relation with an additional term of $\beta_2 [\log_{10}(\sigma/200 \text{ km s}^{-1})]^2$ gives $\beta_2 = 1.52 \pm 1.95$ and does not decrease the intrinsic scatter in M_{\bullet} . Including 92 additional upper limits on M_{\bullet} does not change the fit to the $M_{\bullet} - \sigma$ relation significantly. When the early- and late-type galaxies are fit separately, we obtain nearly identical slopes of ≈ 5 for the $M_{\bullet} - \sigma$ relation but significantly different intercepts. Within early-type galaxies, we find a significantly higher intercept for galaxies with central core profiles than for those with central power-law profiles. At fixed σ , our fits predict M_{\bullet} to be about 2 times higher in early-type galaxies (versus late-type) and 2 times higher in core galaxies (versus power-law). Our $M_{\bullet} - L$ and $M_{\bullet} - M_{\text{bulge}}$ relations for early-type galaxies are similar to those from earlier compilations, and core and power-law galaxies yield similar L - and M_{bulge} -based predictions for M_{\bullet} . Our data set shows evidence for a systematic decrease in the scatter of M_{\bullet} from $\sigma \sim 200 \text{ km s}^{-1}$ to $\sigma \sim 300 \text{ km s}^{-1}$. Galaxies with $L_V < 10^{10} L_{\odot}$ or $M_{\text{bulge}} < 10^{11} M_{\odot}$ exhibit more scatter in M_{\bullet} than galaxies at higher luminosities and bulge masses. Our measurements offer tentative support for theoretical predictions that galaxy merging results in a decreasing intrinsic scatter in M_{\bullet} with increasing galaxy mass.

Subject headings:

1. INTRODUCTION

Empirical correlations between the masses, M_{\bullet} , of supermassive black holes and different properties of their host galaxies have proliferated in the past decade. Power-law fits to these correlations provide efficient means to estimate M_{\bullet} in large samples of galaxies, or in individual objects with insufficient data to measure M_{\bullet} from the dynamics of stars, gas, or masers.

Correlations between black hole masses and numerous properties of their host galaxies have been explored in the literature. These include scaling relations between M_{\bullet} and stellar velocity dispersion (e.g., Ferrarese & Merritt 2000; Gebhardt et al. 2000; Merritt & Ferrarese 2001; Tremaine et al. 2002; Wyithe 2006a,b; Hu 2008; Gültekin et al. 2009a, hereafter G09; Schulze & Gebhardt 2011; McConnell et al. 2011a; Graham et al. 2011; Beifiori et al. 2012, hereafter B12) and between M_{\bullet} and the stellar mass of the bulge (e.g., Magorrian et al. 1998; Marconi & Hunt 2003; Häring & Rix 2004; Hu 2009; Sani et al. 2011; B12). Various scaling relations between M_{\bullet} and the photometric properties of the bulge have also been examined: bulge optical luminosity (e.g., Kormendy & Richstone 1995; Kormendy & Gebhardt 2001; G09; Schulze & Gebhardt 2011; McConnell et al. 2011a; B12), bulge near-infrared luminosity (e.g., Marconi & Hunt 2003; McLure & Dunlop 2002, 2004; Graham 2007; Hu 2009; Sani et al. 2011), total luminos-

ity (e.g., Kormendy & Gebhardt 2001; Kormendy et al. 2011; B12), and bulge concentration or Sérsic index (e.g., Graham et al. 2001; Graham & Driver 2007; B12). On a larger scale, correlations between M_{\bullet} and the circular velocity or dynamical mass of the dark matter halo have been reported as well as disputed (e.g., Ferrarese 2002; Baes et al. 2003; Zasov et al. 2005; Kormendy & Bender 2011; Volonteri et al. 2011; B12). More recently, M_{\bullet} has been found to correlate with the number and total mass of globular clusters in the host galaxy (e.g., Burkert & Tremaine 2010; Harris & Harris 2011; Sadoun & Colin 2012). In core-profile galaxies, Lauer et al. (2007a) and Kormendy & Bender (2009) have explored correlations between M_{\bullet} and the core radius, or the total “light deficit” of the core relative to a Sérsic profile.

Recent kinematic data and modeling efforts have substantially expanded the various samples used in all of the studies above. In this paper, we take advantage of these developments, presenting an updated compilation of 72 black holes and their host galaxies and providing new scaling relations. Our sample is a significant update from two recent compilations by G09 and Graham et al. (2011). Compared with the 49 objects in G09, 25 black holes in our present sample are new measurements, and 18 masses are updated values from better data and/or more sophisticated modeling. Compared with the 64 objects in Graham et al. (2011) (an update of Graham 2008), 35 of our black hole masses are new or updates. The most significant updates in our sample are galaxies with extremely high M_{\bullet} (Shen & Gebhardt 2010; Gebhardt et al. 2011; McConnell et al. 2011b,a, 2012) and

¹ Institute for Astronomy, University of Hawaii at Manoa, Honolulu, HI; nmcc@ifh.hawaii.edu

² Department of Astronomy, University of California at Berkeley, Berkeley, CA; cpma@berkeley.edu

galaxies with some of the smallest observed central black holes (Greene et al. 2010; Nowak et al. 2010; Kormendy et al. 2011; Kuo et al. 2011). The G09 and Graham (2008) samples differ by only a few galaxies, based on the authors’ respective judgments about which dynamical measurements are reliable. Our present sample includes updated distances to 44 galaxies, mostly based on surface brightness fluctuation measurements (Tonry et al. 2001; Blakeslee et al. 2009, 2010).

We focus on the three frequently studied scaling relations: M_\bullet vs. stellar velocity dispersion (σ), V -band bulge luminosity (L), and stellar bulge mass (M_{bulge}). As reported below, our new compilation results in a significantly steeper power law for the $M_\bullet - \sigma$ relation than in G09 and the recent B12 that combined the previous sample of 49 black holes from G09 with a larger sample of upper limits on M_\bullet from Beifiori et al. (2009). We still find a steeper power law when we include these upper limits in our fit to the $M_\bullet - \sigma$ relation. We have performed a quadratic fit to $M_\bullet(\sigma)$ and find a marginal amount of upward curvature, similar to previous investigations (Wyithe 2006a,b; G09).

Another important measurable quantity is the intrinsic or cosmic scatter in M_\bullet for fixed galaxy properties. Quantifying the scatter in M_\bullet is useful for identifying the tightest correlations from which to predict M_\bullet and for testing different scenarios of galaxy and black hole growth. In particular, models of stochastic black hole and galaxy growth via hierarchical merging predict decreasing scatter in M_\bullet as galaxy mass increases (e.g., Peng 2007; Jahnke & Macciò 2011). Previous empirical studies of the black hole scaling relations have estimated the intrinsic scatter in M_\bullet as a single value for the entire sample. Herein, we take advantage of our larger sample to estimate the scatter for multiple bins in σ , L , and M_{bulge} . We find subtle evidence that the black hole scaling relations grow tighter with increasing σ , L , and M_{bulge} .

In §2 we summarize our compilation of 72 black hole mass measurements and an updated compilation of 35 bulge masses from dynamical studies. In §3 we present fits to the $M_\bullet - \sigma$, $M_\bullet - L$, and $M_\bullet - M_{\text{bulge}}$ relations and highlight subsamples that yield interesting variations in the best-fit power laws. In particular, we examine different cuts in σ , L , and M_{bulge} , as well as cuts based on galaxies’ morphologies and surface brightness profiles. In §4 we discuss the scatter in M_\bullet and its dependence on σ , L , and M_{bulge} . In §5 we discuss how our analysis of galaxy subsamples may be beneficial for various applications of the black hole scaling relations.

Our full sample of black hole masses and galaxy properties is available online at <http://blackhole.berkeley.edu>. This database will be updated as new results are published. Investigators are encouraged to use this online database and inform us of updates.

2. AN UPDATED BLACK HOLE AND GALAXY SAMPLE

Our full sample of 72 black hole masses and their host galaxy properties are listed in Table A1, which appears at the end of this paper. We plot the corresponding M_\bullet versus σ , L , and M_{bulge} in Figures 1-3. This sample is an update of our previous compilation of 67 dynamical black

hole measurements, presented in the supplementary materials to McConnell et al. (2011a). The current sample includes one new measurement of M_\bullet from McConnell et al. (2012), seven new measurements from Rusli (2012), and two updated measurements (NGC 4594, Jardel et al. 2011; NGC 3998, Walsh et al. 2012). For NGC 5128 (Cen A), we have adopted the value $M_\bullet = 5.9_{-1.0}^{+1.1} \times 10^7 M_\odot$ (at a distance of 4.1 Mpc) from Cappellari et al. (2009).

We have removed three galaxies whose original measurements have exceptional complications. Lodato & Bertin (2003) measured non-Keplerian maser velocities in NGC 1068 and estimated M_\bullet by modeling a self-gravitating disk. Still, other physical processes might reproduce the observed maser motions. Atkinson et al. (2005) reported a measurement of M_\bullet in NGC 2748 but noted that heavy extinction could corrupt their attempt to locate the center of the nuclear gas disk. Gebhardt et al. (2003) justified classifying the central point source of NGC 7457 as an active galactic nucleus, but their arguments permit the central mass to be shared by an accreting black hole and a nuclear star cluster.

Additionally, we have updated the distances to 44 galaxies in our sample. For 41 galaxies, we adopt surface brightness fluctuation measurements from Tonry et al. (2001) and Blakeslee et al. (2009), with the corrections suggested by Blakeslee et al. (2010). For M31 and M32, we adopt the Cepheid variable distance of 0.73 Mpc from Vilardell et al. (2007). For NGC 4342, we adopt the distance of 23 Mpc from Bogdán et al. (2012). Other measured quantities are scaled accordingly: $M_\bullet \propto D$, $L \propto D^2$, and $M_{\text{bulge}} \propto D$. Table A1 includes the updated values for all quantities. The new galaxy distances and rescaled M_\bullet only have a small effect on our fits to the black hole scaling relations.

For the $M_\bullet - \sigma$ relation, we also consider upper limits for M_\bullet in 89 galaxies from B12, plus 3 new upper limits (Schulze & Gebhardt 2011; Gültekin et al. 2011; McConnell et al. 2012). Five additional galaxies in the B12 upper limit sample have recently obtained secure measurements of M_\bullet and are included in our 72-galaxy sample. As we discuss in §3, including upper limits results in a lower normalization (intercept) for the $M_\bullet - \sigma$ relation but does not significantly alter the slope.

For the $M_\bullet - \sigma$ relation, we consider two different definitions of σ . Both definitions use spatially resolved measurements of the line-of-sight velocity dispersion $\sigma(r)$ and radial velocity $v(r)$, integrated out to one effective radius (r_{eff}):

$$\sigma^2 \equiv \frac{\int_{r_{\text{min}}}^{r_{\text{eff}}} [\sigma^2(r) + v^2(r)] I(r) dr}{\int_{r_{\text{min}}}^{r_{\text{eff}}} I(r) dr}, \quad (1)$$

where $I(r)$ is the galaxy’s one-dimensional stellar surface brightness profile. In G09 and most other studies, the lower integration limit r_{min} is set to zero and sampled at the smallest scale allowed by the data. This definition of σ , however, includes signal from within the black hole radius of influence, $r_{\text{inf}} \equiv GM_\bullet \sigma^{-2}$. In some galaxies, particularly the most massive ellipticals, σ decreases substantially when spatially resolved data within r_{inf} are excluded. Setting $r_{\text{min}} = r_{\text{inf}}$ produces an alternative definition of σ that reflects the global structure of the galaxy and is less sensitive to angular resolution. We compare the two definitions of σ for 12 galaxies whose

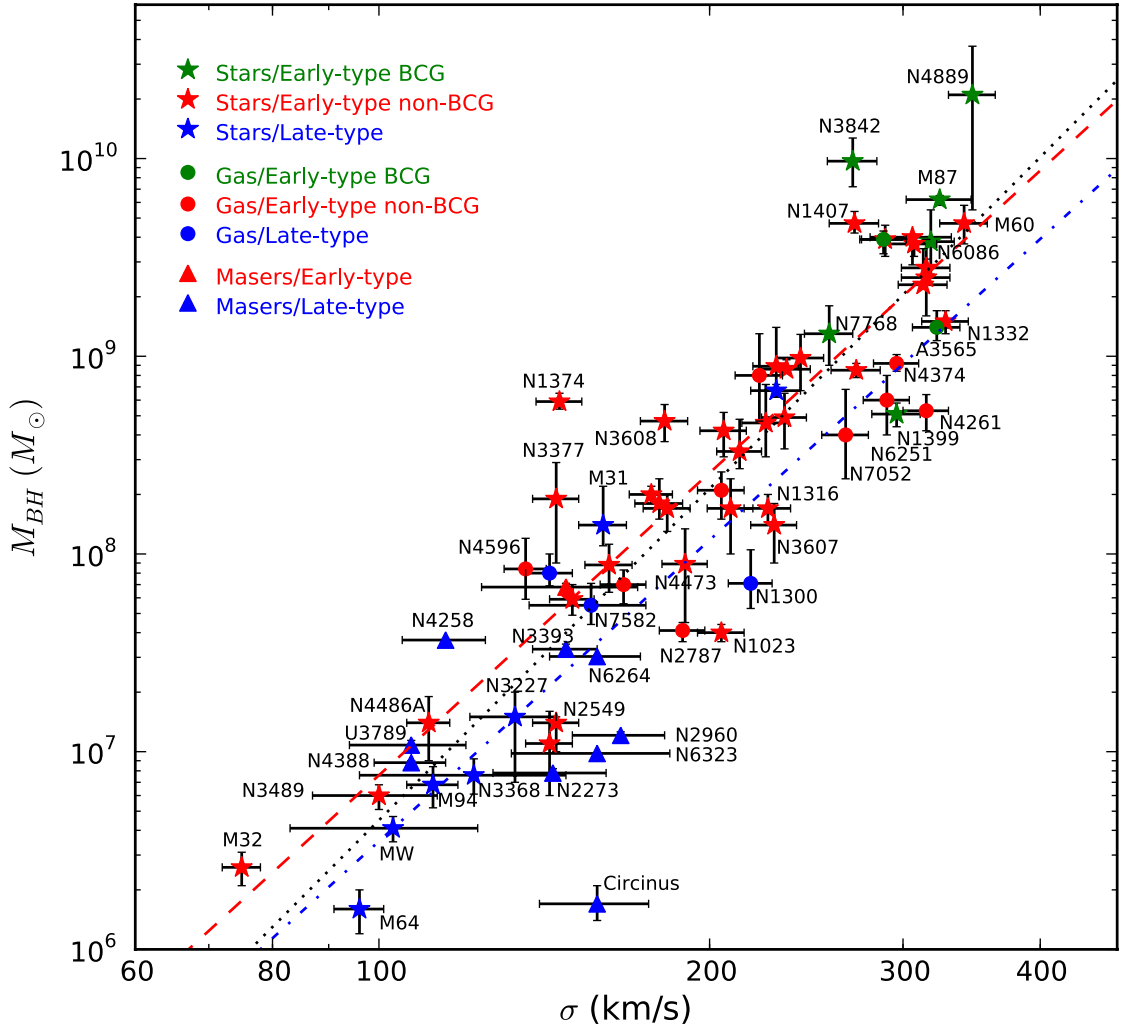


FIG. 1.— The $M_{\bullet} - \sigma$ relation for our full sample of 72 galaxies listed in Table A1 and at <http://blackhole.berkeley.edu>. Brightest cluster galaxies (BCGs) that are also central galaxies of the clusters are plotted in green, other elliptical and S0 galaxies are plotted in red, and late-type spiral galaxies are plotted in blue. For the Fornax Cluster, its BCG NGC 1316 is at the outskirts of the cluster; the green symbol here labels the central galaxy NGC 1399. The black-hole masses are measured using the dynamics of masers (triangles), stars (stars) or gas (circles). Error bars indicate 68% confidence intervals. For most of the maser galaxies, the error bars in M_{\bullet} are smaller than the plotted symbol. The black line shows the best-fitting power law for the entire sample: $\log_{10}(M_{\bullet}/M_{\odot}) = 8.29 + 5.48 \log_{10}(\sigma/200 \text{ km s}^{-1})$. When early-type and late-type galaxies are fit separately, the resulting power laws are $\log_{10}(M_{\bullet}/M_{\odot}) = 8.35 + 5.01 \log_{10}(\sigma/200 \text{ km s}^{-1})$ for the early-type (red line), and $\log_{10}(M_{\bullet}/M_{\odot}) = 8.05 + 5.02 \log_{10}(\sigma/200 \text{ km s}^{-1})$ for the late-type (blue line). The plotted values of σ are derived using kinematic data over the radii $r_{\text{inf}} < r < r_{\text{eff}}$.

kinematics within r_{inf} are notably different from kinematics at larger radii. As shown in Table 1, excluding $r < r_{\text{inf}}$ can reduce σ by up to 10-15%. Ten of the 12 updated galaxies are massive ($\sigma > 250 \text{ km s}^{-1}$ using either definition).

For the $M_{\bullet} - M_{\text{bulge}}$ relation, we have compiled the bulge stellar masses for 35 early-type galaxies. Among them, 13 bulge masses are taken from Häring & Rix (2004), who used spherical Jeans models to fit stellar kinematics. For 22 more galaxies, we multiply the V -band luminosity in Table A1 with the bulge mass-to-light ratio (M/L) derived from kinematics and dynamical modeling of stars or gas (see Table A1 for references). Where necessary, M/L is converted to V -band using galaxy colors. The values of M_{bulge} are scaled to reflect the assumed distances in Table A1.

Most of the dynamical models behind our compiled val-

ues of M_{bulge} have assumed that mass follows light. This assumption can be appropriate in the inner regions of galaxies, where dark matter does not contribute significantly to the total enclosed mass. Still, several measurements are based on kinematic data out to large radii. Furthermore, some galaxies exhibit contradictions between the dynamical estimates of M/L and estimates of M/L from stellar population synthesis models (e.g., Cappellari et al. 2006; Conroy & van Dokkum 2012). For this reason, we adopt a conservative approach and assign a minimum error of 0.24 dex to each value of M_{bulge} . The corresponding confidence interval (0.58 - 1.74) $\times M_{\text{bulge}}$ spans a factor of 3. To test how well our M_{bulge} values represent the stellar mass of each galaxy, we also have fit the $M_{\bullet} - M_{\text{bulge}}$ relation using a sample of 18 galaxies for which M_{bulge} is computed from the stellar mass-to-light ratio, M_{\star}/L . Our fits using the dynamical M_{bulge} and

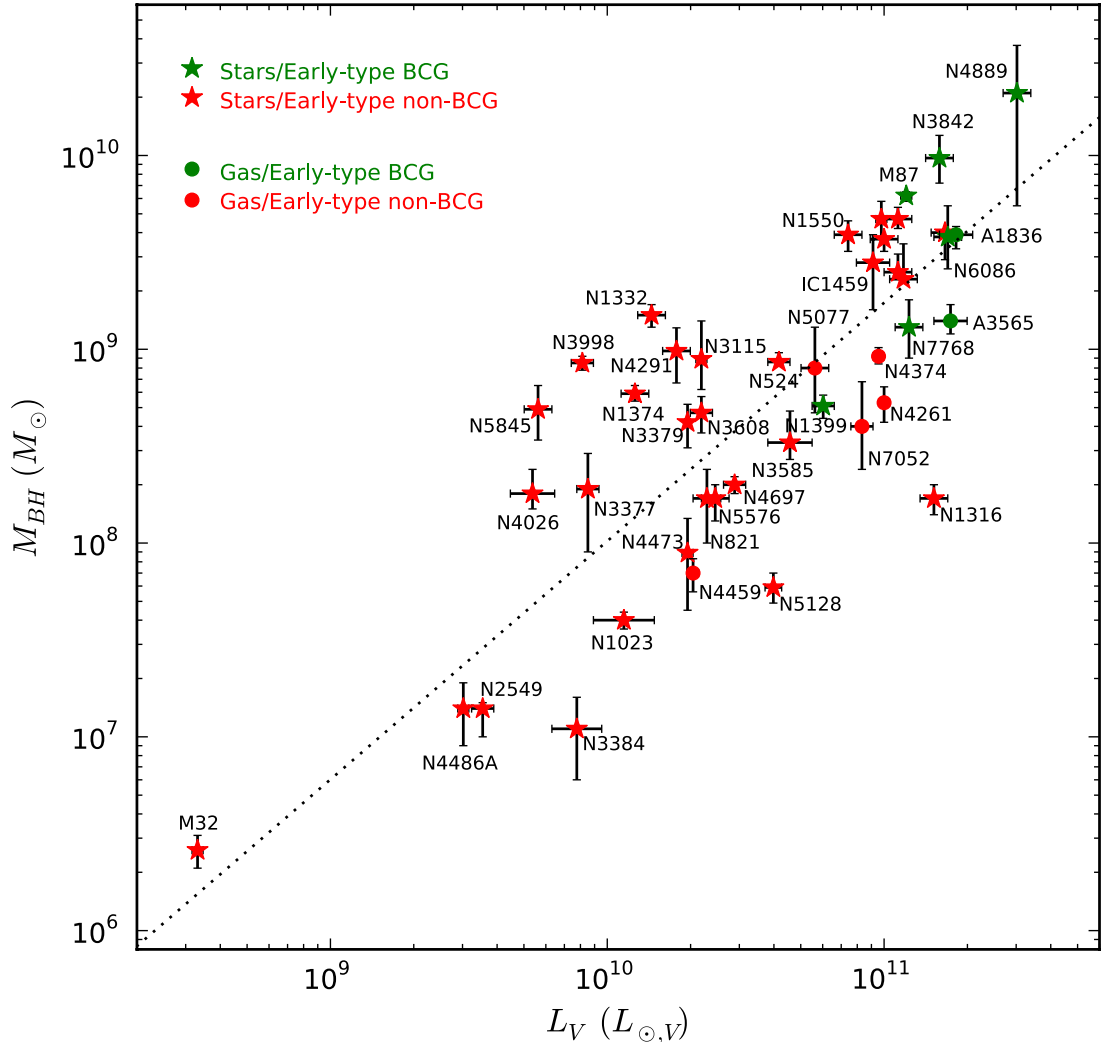


FIG. 2.— The $M_{\bullet} - L$ relation for the X early-type galaxies with reliable measurements of the V-band bulge luminosity in our sample. The symbols are the same as in Figure 1. The black line represents the best-fitting power-law $\log_{10}(M_{\bullet}/M_{\odot}) = 9.18 + 1.24 \log_{10}(L_V/10^{11} L_{\odot})$.

stellar M_{bulge} samples are consistent.

3. BLACK HOLE SCALING RELATIONS AND FITS

In this section we present results for the fits to black hole scaling relations for the full sample of dynamically measured M_{\bullet} listed in Table A1, the full sample of M_{\bullet} plus 92 upper limits on M_{\bullet} , and various subsamples divided by galaxy properties.

3.1. Fitting methods

Our power law fit to a given sample is defined in log space by an intercept α and slope β :

$$\log_{10} M_{\bullet} = \alpha + \beta \log_{10} X, \quad (2)$$

where M_{\bullet} is in units of M_{\odot} , and $X = \sigma/200 \text{ km s}^{-1}$, $L/10^{11} L_{\odot}$, or $M_{\text{bulge}}/10^{11} M_{\odot}$ for the three scaling relations. We have also tested a log-quadratic fit for the $M_{\bullet} - \sigma$ relation:

$$\log_{10} M_{\bullet} = \alpha + \beta \log_{10} X + \beta_2 [\log_{10} X]^2. \quad (3)$$

where $X = \sigma/200 \text{ km s}^{-1}$. Results for the quadratic fit are discussed separately in Sec. 3.2.6 below.

For the power-law scaling relations, we have compared three linear regression estimators: MPFITEXY, LINMIX_ERR, and BIVAR EM. MPFITEXY is a least-squares estimator by Williams et al. (2010). LINMIX_ERR is a Bayesian estimator by Kelly (2007). Both MPFITEXY and LINMIX_ERR consider measurement errors in two variables and include an intrinsic scatter term, ϵ_0 , in $\log(M_{\bullet})$. LINMIX_ERR can be applied to galaxy samples with upper limits for M_{\bullet} . For the $M_{\bullet} - \sigma$ sample with upper limits, we also use the BIVAR EM algorithm in the ASURV software package by Lavalley et al. (1992), which implements the methods presented in Isobe et al. (1986). The ASURV procedures do not consider measurement errors, and we use this method primarily for comparison with B12. All three algorithms are publicly available³.

For each of the global scaling relations and galaxy subsamples, we obtain consistent fits from MPFITEXY and LINMIX_ERR. Table 2 includes the global fitting results

³ The IDL source code for MPFITEXY is available at <http://purl.org/mike/mpfitexy>. THE IDL source code for LINMIX_ERR and dependent scripts is available at <http://idlastro.gsfc.nasa.gov/ftp/pro/math>. ASURV is available at <http://www2.astro.psu.edu/statcodes/asurv>.

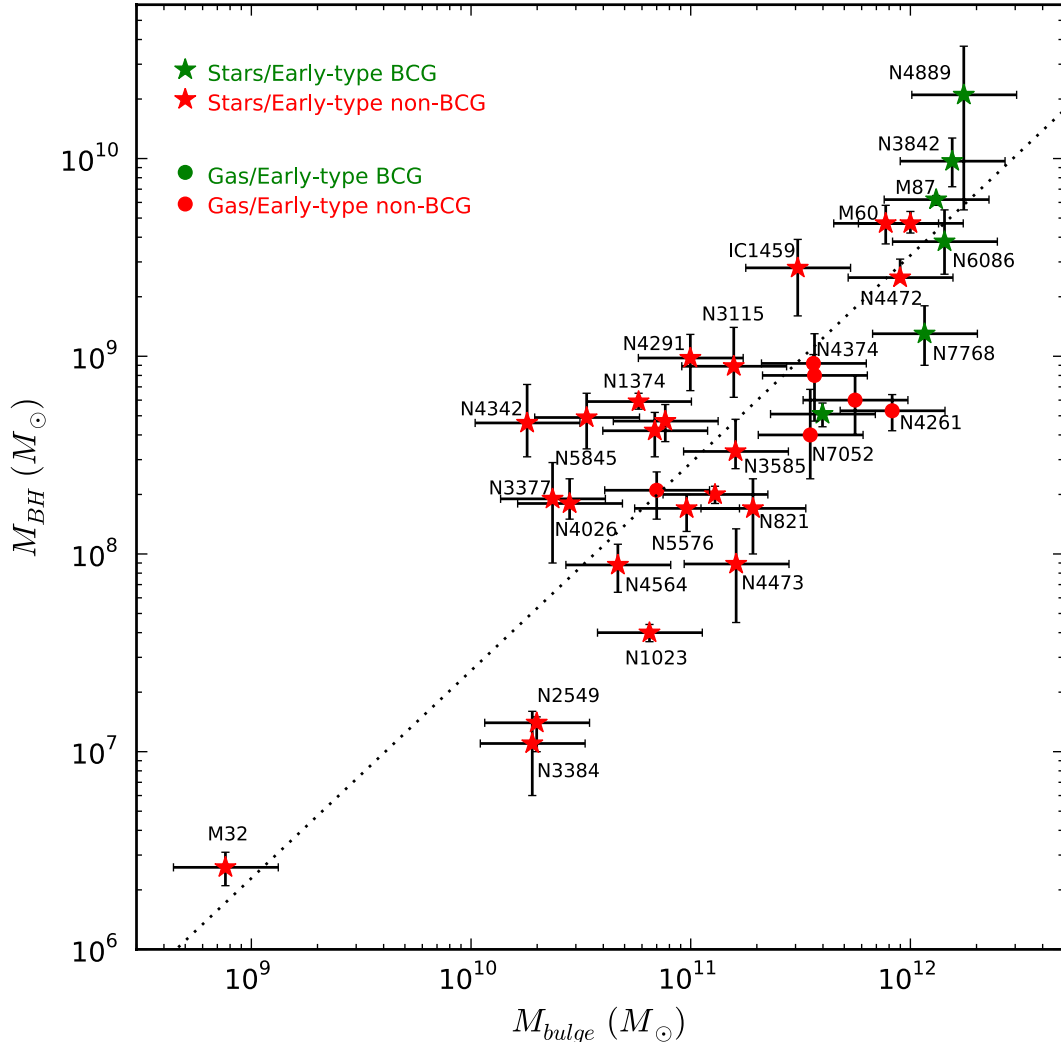


FIG. 3.— The $M_{\bullet} - M_{\text{bulge}}$ relation for the X early-type galaxies with dynamical measurements of the bulge stellar mass in our sample. The symbols are the same as in Figure 1. The black line represents the best-fitting power-law $\log_{10}(M_{\bullet}/M_{\odot}) = 8.42 + 1.07 \log_{10}(M_{\text{bulge}}/10^{11} M_{\odot})$.

from both methods. In Table 2 we also include results from LINMIX_ERR in cases where ϵ_0 is poorly constrained by MPFITEXY. For the $M_{\bullet} - \sigma$ relation including upper limits, we also obtain consistent fits from LINMIX_ERR and ASURV BIVAR EM. Recently, Park et al. (2012) investigated the $M_{\bullet} - \sigma$ relation using four linear regression estimators, including MPFITEXY and LINMIX_ERR. All four estimators yielded consistent fits to empirical data, and MPFITEXY and LINMIX_ERR behaved robustly for simulated data with large measurement errors in σ .

3.2. $M_{\bullet} - \sigma$ Relation

Our fits to $M_{\bullet}(\sigma)$ for the entire galaxy sample and various subsamples are plotted in Figures 1 and 4a, and summarized in Table 2.

3.2.1. Full Sample

Our full sample of 72 galaxies yields an intercept $\alpha = 8.33 \pm 0.05$ and slope $\beta = 5.57 \pm 0.33$. When upper limits are added, the sample of 164 galaxies yields $\alpha = 8.30 \pm 0.06$ and $\beta = 5.67 \pm 0.34$.

3.2.2. Early vs Late Type

Fitting early- and late-type galaxies separately yields slightly shallower slopes of $\beta \approx 5.0$ for both types (red vs blue lines in Figure 1), and the late-type galaxies have a significantly lower intercept: $\alpha = 8.41 \pm 0.06$ versus 8.07 ± 0.21 . Correspondingly, our fits predict $M_{\bullet, \text{early}} \sim 2 M_{\bullet, \text{late}}$ at fixed σ . Because most of the late-type bulges have low σ , the split in intercepts leads to a steeper slope of 5.57 for the full sample.

3.2.3. Core vs Power-law

We also consider two subsamples of early-type galaxies classified by the slopes of their inner surface brightness profiles, $\gamma = -d \log I / d \log r$. Faber et al. (1997) and Lauer et al. (2007b) distinguished “power-law” galaxies with $\gamma > 0.5$ from “core” galaxies with $\gamma < 0.3$, although other studies have reported a continuous trend in γ (e.g., Ferrarese et al. 2006; Glass et al. 2011). Core galaxies tend to be more massive and luminous than power-law galaxies, and there is some evidence that M_{\bullet} correlates with properties of the inner stellar core (Lauer et al.

2007a; Kormendy & Bender 2009). In our fits to $M_{\bullet}(\sigma)$, core galaxies have a significantly higher intercept than power-law galaxies (see Figure 4a): $\alpha = 8.60 \pm 0.11$ versus 8.24 ± 0.09 . Our fits predict $M_{\bullet,\text{core}} \sim 2 M_{\bullet,\text{pl}}$ at fixed σ . The offset in intercepts plus the shallower slopes ($\beta \sim 4.5$) for core and power-law galaxies combine to produce a steeper slope ($\beta \approx 5$) for the early-type $M_{\bullet} - \sigma$ relation.

3.2.4. Definitions of σ

As discussed in §2, the value of σ for each galaxy used in the $M_{\bullet} - \sigma$ relation depends on the spatial extent of the kinematic data. Excluding data within r_{inf} (when resolved) has the effect of decreasing σ and increasing the slope of the $M_{\bullet} - \sigma$ relation. We have obtained new values of σ for 12 galaxies in our sample by examining kinematic profiles from the literature and excluding data within r_{inf} ; these galaxies are listed in Table 1. Ten of the 12 galaxies have $\sigma > 250 \text{ km s}^{-1}$ using either definition.

In Table 2 we test how much the definition of σ affects our fit to our full sample of 72 galaxies, as well as subsamples dominated by massive early-type galaxies (see rows labeled “0- r_{eff} ”). We find the slope of the global $M_{\bullet} - \sigma$ relation to change slightly from $\beta = 5.57 \pm 0.33$ in our fiducial sample (in which $\sigma(r_{\text{inf}} - r_{\text{eff}})$ is used) to $\beta = 5.44 \pm 0.30$ for the conventional definition of σ with $r_{\text{min}} = 0$ in Equation (1). The latter is a fairer quantity to be compared with earlier studies, but the resulting $M_{\bullet} - \sigma$ relation is still significantly steeper than those reported in G09 and B12. The definition of σ does not significantly affect our measurements of the intrinsic scatter in $\log(M_{\bullet})$ (see Table 2 and §4).

3.2.5. High vs Low σ

To search for possible systematic deviations of the $M_{\bullet} - \sigma$ relation from a single power law, we divide the galaxies into low- σ and high- σ subsamples, separated by a cutoff value σ_{cut} . We have tested numerous values of σ_{cut} and found two robust trends. First, for σ_{cut} in the

TABLE 1
GALAXIES WITH MULTIPLE DEFINITIONS OF σ

Galaxy	Ref.	r_{inf} (")	σ (0- r_{eff}) (km s^{-1})	σ ($r_{\text{inf}} - r_{\text{eff}}$) (km s^{-1})
IC 1459	1	0.8	340	315
NGC 1374	2	1.3	167	146
NGC 1399	3,4	0.6	337	296
NGC 1407	5	1.9	283	274
NGC 1550	6	0.78	302	289
NGC 3842	7	1.2	275	270
NGC 3998	8	0.7	286	272
NGC 4486	9	2.1	375	324
NGC 4594	10	1.2	240	230
NGC 4649	11	2.2	385	341
NGC 4889	7	1.5	360	347
NGC 7619	12	0.39	324	313
NGC 7768	7	0.14	265	257

Notes: References for kinematic data used to derive r_{inf} are (1) Cappellari et al. 2002; (2) Rusli 2012; (3) Graham et al. 1998; (4) Gebhardt et al. 2007; (5) Spolaor et al. 2008; (6) Simien & Prugniel 2000; (7) McConnell et al. 2012; (8) Walsh et al. 2012; (9) Gebhardt et al. 2011; (10) Jardel et al. 2011; (11) Pinkney et al. 2003; (12) Pu et al. 2010.

range $175\text{--}225 \text{ km s}^{-1}$, the higher- σ sample exhibits a steeper slope ($\beta \sim 6\text{--}7$) than the lower- σ sample ($\beta \sim 5$). Still, the differences between the fits for the two subsamples are within 1σ error bars as the uncertainties in α and β are large. As an example, Table 2 lists the fitting results for $\sigma_{\text{cut}} = 200 \text{ km s}^{-1}$. Second, the relation for the higher- σ sample appears to steepen drastically when $\sigma_{\text{cut}} \gtrsim 270 \text{ km s}^{-1}$. As shown in Table 2 (for $\sigma_{\text{cut}} = 275 \text{ km s}^{-1}$), the MPFITEXY and LINMIX_ERR procedures both return nearly vertical relations, with very large uncertainties in β . This suggests a breakdown of the $M_{\bullet} - \sigma$ correlation as the galaxy population “sat-

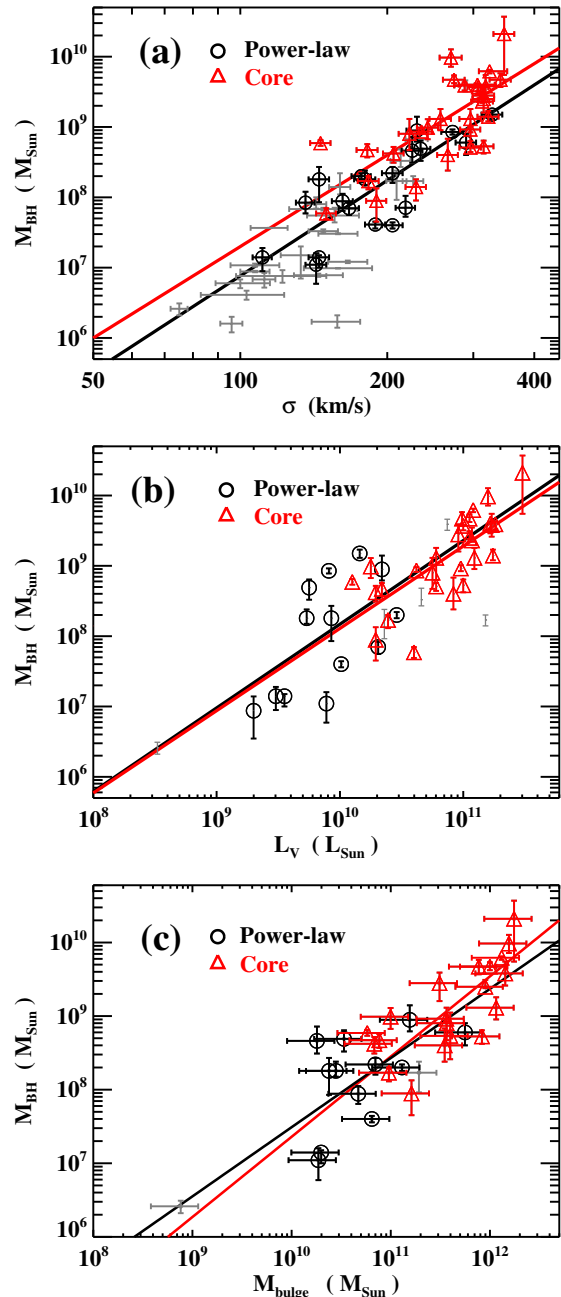


FIG. 4.— Black hole scaling relations, with separate fits for power-law galaxies (solid black lines), versus core galaxies (dashed red lines). (a) $M_{\bullet} - \sigma$ relation. (b) $M_{\bullet} - L$ relation. (c) $M_{\bullet} - M_{\text{bulge}}$ relation.

urates” at $\sigma \sim 350 \text{ km s}^{-1}$. Saturation of the $L - \sigma$ and $M_{\bullet} - \sigma$ relations has been predicted from observations and simulations of the most massive galaxies (e.g., Boylan-Kolchin et al. 2006; Bernardi et al. 2007; Lauer et al. 2007a). The MPFITEXY procedure returns zero intrinsic scatter when fitting galaxies with $\sigma > 275 \text{ km s}^{-1}$; this is an artifact of the large slope.

One might suspect that the saturation in $M_{\bullet}(\sigma)$ results from the lower σ values we obtained for 12 galaxies after excluding data within r_{inf} . We have also fit the high- σ and low- σ subsamples using the conventional definition of σ . We still find that the highest- σ galaxies follow a very steep $M_{\bullet} - \sigma$ relation, although this trend begins to appear at slightly higher values of σ_{cut} (exemplified by $\sigma_{\text{cut}} = 290 \text{ km s}^{-1}$ in Table 2).

It is tempting to fit $M_{\bullet}(\sigma)$ for narrow intervals in σ (e.g., $150 \text{ km s}^{-1} < \sigma < 200 \text{ km s}^{-1}$), but the intrinsic scatter in the $M_{\bullet} - \sigma$ relation drives these samples toward an uncorrelated distribution. For the current sample of M_{\bullet} , a long baseline in σ ($\gtrsim 100 \text{ km s}^{-1}$) is therefore needed to determine the slope of the $M_{\bullet} - \sigma$ relation.

We have also tried fitting $M_{\bullet}(\sigma)$ for subsamples defined by cuts in L and M_{bulge} ; two examples are listed in Table 2. Some of the high- L subsamples exhibit a steep $M_{\bullet} - \sigma$ slope, but again with large uncertainties.

3.2.6. A Log-quadratic Fit to $M_{\bullet} - \sigma$

In light of evidence that the $M_{\bullet} - \sigma$ relation steepens toward high galaxy masses, we have also attempted to fit $M_{\bullet}(\sigma)$ as a log-quadratic function in Equation (3). The coefficients α , β , β_2 , and intrinsic scatter ϵ_0 for our 72-galaxy sample are determined from a brute-force least-squares estimator similar to MPFITEXY. We find that the best-fit parameters are $\alpha = 8.28 \pm 0.08$, $\beta = 5.70 \pm 0.35$, $\beta_2 = 1.52 \pm 1.95$, and $\epsilon_0 = 0.40$. Uncertainties in α , β , and β_2 are determined by assessing the one-dimensional likelihood function after marginalizing χ^2 with respect to the other two parameters. We find $\beta_2 > 0$ with 79% confidence, slightly below the 1σ threshold for a one-sided confidence interval.

As suggested by the highly uncertain power-law slopes for high- σ galaxies, our measurement of upward curvature in $M_{\bullet}(\sigma)$ is marginal. Adopting a quadratic relation does not decrease the intrinsic scatter in M_{\bullet} . Our full sample updates the investigations of Wyithe (2006a,b; 31 galaxies) and G09 (49 galaxies), who reported similar confidence levels for a non-zero quadratic term. At the extreme end of the local galaxy velocity dispersion function ($\sigma \sim 400 \text{ km s}^{-1}$), our best quadratic fit predicts black hole masses $\sim 40\%$ higher than the best power-law fit.

3.3. $M_{\bullet} - L$ and $M_{\bullet} - M_{\text{bulge}}$ Relations

In Table A1, we present V -band luminosities for 44 galaxies and dynamically measured bulge masses for 35 galaxies. For several of the late-type galaxies in our sample, the literature contains one or more estimates of the bulge-to-total light ratio. Rather than judging between the various estimates, we present results for the early-types only. Our best fit values are $\beta = 1.11 \pm 0.13$ and $\alpha = 9.23 \pm 0.10$ for the $M_{\bullet} - L$ relation, and $\beta = 1.05 \pm 0.11$ and $\alpha = 8.46 \pm 0.08$ for the $M_{\bullet} - M_{\text{bulge}}$ relation.

Additional fits to subsamples of these galaxies are listed in Table 2. The $M_{\bullet} - L$ and $M_{\bullet} - M_{\text{bulge}}$ relations do not show statistically significant differences between core and power-law galaxies (see also Figs. 4b and 4c).

Figures 2 and 3 show that our $M_{\bullet} - L$ and $M_{\bullet} - M_{\text{bulge}}$ samples both appear to have a central knot, where black holes with $10^8 M_{\odot} < M_{\bullet} < 10^9 M_{\odot}$ exhibit relatively weak correlation with L or M_{bulge} . This feature makes it difficult to interpret the fits to high- L and low- L (or high- M_{bulge} and low- M_{bulge}) subsamples. We find tentative evidence that the most luminous and massive galaxies ($L > 10^{10.8} L_{\odot}$; $M_{\text{bulge}} > 10^{11.5} M_{\odot}$) have steeper slopes in $M_{\bullet}(L)$ and $M_{\bullet}(M_{\text{bulge}})$, as exemplified in Table 2. Both samples are sparsely populated at the low- M_{\bullet} end.

3.4. Comparison to Previous Studies

The slope of the $M_{\bullet} - \sigma$ relation reported in prior studies has wavered between ~ 4 (e.g., Gebhardt et al. 2000; Tremaine et al. 2002; G09; B12) and ~ 5 (e.g., Ferrarese & Merritt 2000; Merritt & Ferrarese 2001; Graham et al. 2011). Our best-fit slope for the global $M_{\bullet} - \sigma$ relation falls at the steep end of this distribution, while various subsamples exhibit a wider range of slopes ($\beta \approx 3.8$ to $\beta > 12$). In particular, the $M_{\bullet} - \sigma$ relation for our full sample is significantly steeper than those reported in G09 ($\beta = 4.24 \pm 0.41$) and B12 ($\beta = 4.42 \pm 0.30$).

Our fit to early-type galaxies is significantly steeper than the early-type fit by G09 ($\beta = 5.08 \pm 0.38$, versus $\beta = 3.96 \pm 0.42$). This difference is due to several changes to the high- σ galaxy sample, e.g., new measurements of $M_{\bullet} \sim 10^{10} M_{\odot}$ in the brightest cluster galaxies NGC 4889 and NGC 3842 (McConnell et al. 2011a), updated measurements increasing M_{\bullet} in M87 and M60 (Gebhardt & Thomas 2009; Shen & Gebhardt 2010), and our definition of σ to exclude the black hole radius of influence. Our fit for late-type galaxies is slightly steeper than G09 ($\beta = 5.02 \pm 1.18$, versus $\beta = 4.58 \pm 1.58$). This arises primarily from our exclusion of NGC 1068 and NGC 2748.

Our earlier compilation of a similar sample of 67 galaxies (McConnell et al. 2011a) gave $\alpha = 8.28 \pm 0.06$ and $\beta = 5.13 \pm 0.34$ for the $M_{\bullet} - \sigma$ relation. Our $M_{\bullet}(\sigma)$ fit to the present sample of 72 galaxies has a steeper slope of 5.57 ± 0.33 , largely due to the exclusion of NGC 7457, which had the lowest velocity dispersion ($\sigma = 67 \text{ km s}^{-1}$) of all galaxies in the previous sample (see § 2 and Gebhardt et al. 2003 for discussion of this galaxy’s central massive object).

Our $M_{\bullet} - L$ and $M_{\bullet} - M_{\text{bulge}}$ slopes are consistent with a number of previous investigations, including multiple bandpasses for L (e.g., Marconi & Hunt 2003; Häring & Rix 2004; McLure & Dunlop 2004; G09; Schulze & Gebhardt 2011). Some differences should be noted, however. For the $M_{\bullet} - L$ relation, Sani et al. (2011) report different $M_{\bullet} - L_{3.6\mu\text{m}}$ and $M_{\bullet} - L_V$ slopes and suggest that color corrections and extinction may be responsible for the difference. Their $M_{\bullet} - L_{3.6\mu\text{m}}$ slope is 0.93 ± 0.10 ; their $M_{\bullet} - L_V$ slope ranges from 1.11 to 1.40 depending on the regression method, and is consistent with our $M_{\bullet} - L_V$ slope of 1.11 ± 0.13 .

For the $M_{\bullet} - M_{\text{bulge}}$ relation, the latest compilation of 46 galaxies by B12 gives a slope of 0.79 ± 0.26 . We note that their M_{bulge} values are virial estimates based on the galaxies’ σ and r_{eff} via $M_{\text{bulge}} = 5.0\sigma^2 r_{\text{eff}}/G$. In comparison, our M_{bulge} values use the mass-to-light

TABLE 2
POWER-LAW FITS TO BLACK HOLE CORRELATIONS

Sample	N_{gal}	Method	α	β	ϵ_0
$M_{\bullet} - \sigma$ relation					
All galaxies	72	MPFITEXY	8.33 ± 0.05	5.57 ± 0.33	0.40
All galaxies	72	LINMIX_ERR	8.32 ± 0.06	5.58 ± 0.34	0.42 ± 0.04
All + upper limits	164	LINMIX_ERR	8.30 ± 0.06	5.67 ± 0.34	0.42 ± 0.04
All galaxies ($0 - r_{\text{eff}}$)	72	MPFITEXY	8.30 ± 0.05	5.44 ± 0.30	0.38
G09 data ($0 - r_{\text{eff}}$)	49	MPFITEXY	8.19 ± 0.06	4.12 ± 0.38	0.39
Early-type	53	MPFITEXY	8.41 ± 0.06	5.08 ± 0.38	0.36
Early-type ($0 - r_{\text{eff}}$)	53	MPFITEXY	8.38 ± 0.06	4.97 ± 0.35	0.34
Late-type	19	MPFITEXY	8.07 ± 0.21	5.06 ± 1.16	0.46
Power-law	18	MPFITEXY	8.24 ± 0.09	4.51 ± 0.73	0.34
Core	28	MPFITEXY	8.60 ± 0.11	4.32 ± 0.74	0.38
Core ($0 - r_{\text{eff}}$)	28	MPFITEXY	8.55 ± 0.11	4.30 ± 0.68	0.36
$\sigma \leq 200 \text{ km s}^{-1}$	35	MPFITEXY	8.32 ± 0.17	5.41 ± 0.91	0.46
$\sigma > 200 \text{ km s}^{-1}$	37	MPFITEXY	8.16 ± 0.13	6.76 ± 0.91	0.34
$\sigma > 200 \text{ km s}^{-1}$ ($0 - r_{\text{eff}}$)	37	MPFITEXY	8.21 ± 0.12	5.99 ± 0.80	0.34
$\sigma \leq 275 \text{ km s}^{-1}$	55	LINMIX_ERR	8.33 ± 0.08	5.66 ± 0.52	0.45 ± 0.06
$\sigma > 275 \text{ km s}^{-1}$	17	LINMIX_ERR	7.00 ± 2.42	12.3 ± 12.6	0.34 ± 0.11
$\sigma > 275 \text{ km s}^{-1}$	17	MPFITEXY	2.47 ± 3.17	35.8 ± 16.5	N/A
$\sigma > 290 \text{ km s}^{-1}$ ($0 - r_{\text{eff}}$)	15	LINMIX_ERR	7.68 ± 1.26	7.93 ± 5.79	0.32 ± 0.11
$L \leq 10^{10.8} L_{\odot}$	25	MPFITEXY	8.38 ± 0.08	4.53 ± 0.60	0.37
$L > 10^{10.8} L_{\odot}$	19	MPFITEXY	8.13 ± 0.40	7.19 ± 2.25	0.37
$L > 10^{10.8} L_{\odot}$ ($0 - r_{\text{eff}}$)	19	MPFITEXY	8.29 ± 0.33	5.83 ± 1.75	0.36
$M_{\text{bulge}} \leq 10^{11.5} M_{\odot}$	21	MPFITEXY	8.41 ± 0.10	4.76 ± 0.77	0.39
$M_{\text{bulge}} > 10^{11.5} M_{\odot}$	14	MPFITEXY	8.52 ± 0.47	4.69 ± 2.69	0.46
$M_{\text{bulge}} > 10^{11.5} M_{\odot}$ ($0 - r_{\text{eff}}$)	14	MPFITEXY	8.61 ± 0.40	3.80 ± 2.09	0.45
$M_{\bullet} - L$ relation					
Early-type galaxies	44	MPFITEXY	9.23 ± 0.10	1.11 ± 0.13	0.49
Early-type galaxies	44	LINMIX_ERR	9.23 ± 0.10	1.11 ± 0.14	0.52 ± 0.06
G09 data (early-type)	32	MPFITEXY	9.01 ± 0.10	1.17 ± 0.12	0.36
Power-law	12	MPFITEXY	9.36 ± 0.72	1.19 ± 0.67	0.68
Core	27	MPFITEXY	9.28 ± 0.09	1.17 ± 0.22	0.39
$L \leq 10^{10.8} L_{\odot}$	25	MPFITEXY	9.10 ± 0.23	0.98 ± 0.20	0.54
$L > 10^{10.8} L_{\odot}$	19	MPFITEXY	9.27 ± 0.13	1.12 ± 0.82	0.47
$M_{\text{bulge}} \leq 10^{11.5} M_{\odot}$	18	MPFITEXY	9.25 ± 0.24	1.13 ± 0.23	0.47
$M_{\text{bulge}} > 10^{11.5} M_{\odot}$	13	MPFITEXY	9.24 ± 0.10	2.49 ± 0.67	0.30
$M_{\bullet} - M_{\text{bulge}}$ relation					
Dynamical masses	35	MPFITEXY	8.46 ± 0.08	1.05 ± 0.11	0.34
Dynamical masses	35	LINMIX_ERR	8.46 ± 0.09	1.05 ± 0.12	0.36 ± 0.08
Stellar masses	18	MPFITEXY	8.55 ± 0.12	1.23 ± 0.16	0.31
Power-law	12	MPFITEXY	8.43 ± 0.20	0.94 ± 0.39	0.50
Core	20	MPFITEXY	8.45 ± 0.15	1.09 ± 0.20	0.28
$L \leq 10^{10.8} L_{\odot}$	19	LINMIX_ERR	8.44 ± 0.14	1.05 ± 0.26	0.45 ± 0.13
$L > 10^{10.8} L_{\odot}$	12	LINMIX_ERR	7.66 ± 1.60	1.92 ± 1.72	0.38 ± 0.19
$L > 10^{10.8} L_{\odot}$	12	FITEXY	6.92 ± 1.05	2.72 ± 1.12	N/A
$M_{\text{bulge}} \leq 10^{11.5} M_{\odot}$	21	LINMIX_ERR	8.54 ± 0.15	1.11 ± 0.28	0.47 ± 0.12
$M_{\text{bulge}} > 10^{11.5} M_{\odot}$	14	LINMIX_ERR	7.28 ± 1.19	2.26 ± 1.33	0.30 ± 0.17
$M_{\text{bulge}} > 10^{11.5} M_{\odot}$	14	FITEXY	0 ± 0	0 ± 0	N/A

Notes: For the $M_{\bullet} - \sigma$ relation, we fit $\log(M_{\bullet}) = \alpha + \beta \log(\sigma/200 \text{ km s}^{-1})$. Subsamples designated ($0 - r_{\text{eff}}$) define σ using kinematic data over the interval $0 < r < r_{\text{eff}}$. For all other subsamples, we define σ using data over the interval $r_{\text{inf}} < r < r_{\text{eff}}$. For the $M_{\bullet} - L$ relation, we fit $\log_{10} M_{\bullet} = \alpha + \beta \log_{10}(L/10^{11} L_{\odot})$. Luminosities are in V-band. For the $M_{\bullet} - M_{\text{bulge}}$ relation, we fit $\log_{10} M_{\bullet} = \alpha + \beta \log_{10}(M_{\text{bulge}}/10^{11} M_{\odot})$. All fits except for the “stellar masses” line use the sample of bulges with dynamical masses.

ratios obtained from dynamical models.

Recently, Graham (2012) examined the $M_\bullet - \sigma$ and $M_\bullet - M_{\text{bulge}}$ relations with separate fits to core and non-core galaxies, based on the galaxy sample of Häring & Rix (2004) and updated black hole masses from Graham et al. (2011). The non-core galaxies were found to follow a very steep $M_\bullet - M_{\text{bulge}}$ relation ($\beta \sim 2$), and there was virtually no difference in the $M_\bullet - \sigma$ relations for core versus non-core galaxies. Our relative trends for core and power-law galaxies differ from those in Graham (2012). This is likely due to differences in the galaxy samples: our core galaxies include eight galaxies with $M_\bullet > 10^9 M_\odot$, which are absent from the sample of Graham (2012). Our photometric classification of galaxies also differs from Graham (2012). In particular, we classify the high- M_{bulge} object NGC 6251 as a power-law galaxy, based on the surface brightness profile of Ferrarese & Ford (1999). Excluding NGC 6251, we measure update this: $\beta \approx 1.7$ for power-law galaxies on the $M_\bullet - M_{\text{bulge}}$ relation.

4. SCATTER IN BLACK HOLE MASS

For a given black hole scaling relation, deviations between the measured values of M_\bullet and the mean power-law relation are conventionally interpreted as a combination of measurement errors and intrinsic scatter. We assume the scatter in M_\bullet to be log normal, and define the intrinsic scatter term ϵ_0 such that

$$\chi^2 = \sum_i \frac{[\log(M_{\bullet,i}) - \alpha - \beta x_i]^2}{\epsilon_0^2 + \epsilon_{M,i}^2 + \beta^2 \epsilon_{x,i}^2}, \quad (4)$$

where $x = \log_{10}(\sigma/200 \text{ km s}^{-1})$ for the $M_\bullet - \sigma$ relation, $x = \log_{10}(L/10^{11} L_\odot)$ for the $M_\bullet - L$ relation, and $x = \log_{10}(M_{\text{bulge}}/10^{11} M_\odot)$ for the $M_\bullet - M_{\text{bulge}}$ relation. Here, ϵ_M is the 1- σ error in $\log(M_\bullet)$, and ϵ_x is the 1- σ error in x . For a given sample and power-law fit, we adopt the value of ϵ_0 for which $\chi_\nu^2 = 1$ ($\chi^2 = N_{\text{dof}}$). G09 tested several forms of intrinsic scatter in M_\bullet and found log normal scatter to be an appropriate description.

Fitting the full galaxy sample for each scaling relation, we find the intrinsic scatter in $\log_{10}(M_\bullet)$ to be $\epsilon_0 = 0.40$ for the $M_\bullet - \sigma$ relation, $\epsilon_0 = 0.49$ for the $M_\bullet - L$ relation, and $\epsilon_0 = 0.34$ for the $M_\bullet - M_{\text{bulge}}$ relation. While it is tempting to conclude that M_{bulge} is the superior predictor of M_\bullet , the relative errors in M_{bulge} , σ , and L demand a more cautious interpretation. As noted in §2, we have assumed that all M_{bulge} values have an error of at least 0.24 dex. We have repeated our fits to $M_\bullet(M_{\text{bulge}})$ with a minimum error of only 0.09 dex. Fitting the full M_{bulge} sample with this reduced error in M_{bulge} , we obtain a larger intrinsic scatter ($\epsilon_0 = 0.39$) as expected from equation (4), while the slope and intercept of the fit remain unchanged. Similarly, our measurements of ϵ_0 for the $M_\bullet - \sigma$ and $M_\bullet - L$ relations depend in part upon the assumed errors in σ ($\geq 5\%$, following G09) and L (typically < 0.05 dex).

Beyond the intrinsic scatter ϵ_0 in black hole mass for the full sample, the dependence of ϵ_0 on σ , L , and M_{bulge} is a useful quantity for constraining theoretical models of black hole assembly. Successive mergers are predicted to drive galaxies toward the mean $M_\bullet - M_{\text{bulge}}$ relation, especially when black hole growth is dominated by black hole-black hole mergers (e.g., Peng 2007; Jahnke

& Macciò 2011). Understanding intrinsic scatter in M_\bullet is also crucial for estimating the mass function of black holes, starting from the luminosity function or velocity dispersion function of galaxies (e.g., Lauer et al. 2007c;

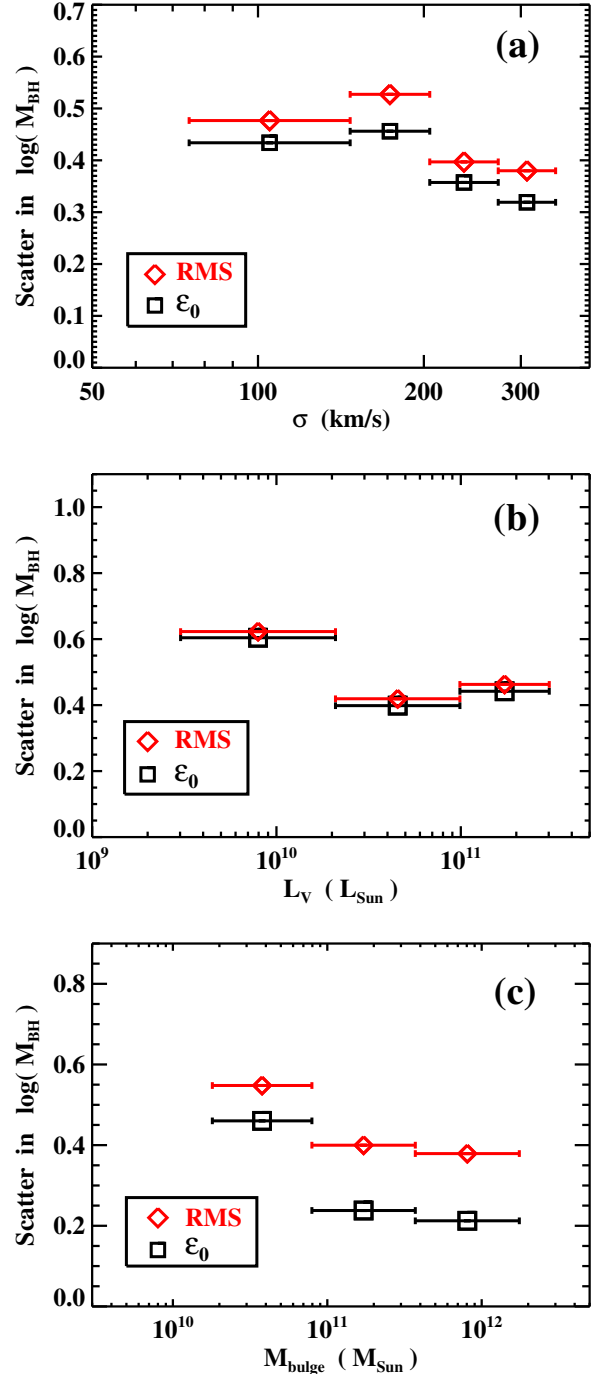


FIG. 5.— Scatter in $\log_{10} M_\bullet$ for different intervals in σ , L , and M_{bulge} . For each interval, ϵ_0 is the intrinsic scatter required to obtain $\chi^2 = N_{\text{gal}}$ between the subsample of galaxies and the global power law. RMS is the root-mean-squared scatter in $\log_{10} M_\bullet$ for each interval. (a) Scatter with respect to the $M_\bullet - \sigma$ relation, $\log_{10} M_\bullet = 8.29 + 5.48 \log_{10}(\sigma/200 \text{ km s}^{-1})$. (b) Scatter with respect to the $M_\bullet - L$ relation, $\log_{10} M_\bullet = 9.18 + 1.24 \log_{10}(L/10^{11} L_\odot)$. (c) Scatter with respect to the $M_\bullet - M_{\text{bulge}}$ relation, $\log_{10} M_\bullet = 8.42 + 1.07 \log_{10}(M_{\text{bulge}}/10^{11} M_\odot)$.

G09).

Figure 5 illustrates how ϵ_0 varies across each of the $M_\bullet - \sigma$, $M_\bullet - L$, and $M_\bullet - M_{\text{bulge}}$ relations for our updated sample of measurements. For each relation, we construct three or four bins containing equal numbers of galaxies and compute ϵ_0 in each bin. The same values of α and β are used for all bins, representing the global fit to the appropriate scaling relation.

The intrinsic scatter illustrated in Figure 5a shows a subtle decrease, from $\epsilon_0 \approx 0.45$ for galaxies with $\sigma < 200 \text{ km s}^{-1}$ to $\epsilon_0 \sim 0.3$ for galaxies with $\sigma \sim 300 \text{ km s}^{-1}$. For the $M_\bullet - L$ and $M_\bullet - M_{\text{bulge}}$ relations, we find possible evidence that galaxies with low spheroid luminosities ($L \lesssim 10^{10} L_\odot$) and small stellar masses ($M_{\text{bulge}} \lesssim 10^{11} M_\odot$) exhibit increased intrinsic scatter in M_\bullet . Yet the scatter appears constant for galaxies above this range, spanning $10^{10} L_\odot \lesssim L \lesssim 10^{11.5} L_\odot$ and $10^{11} M_\odot \lesssim M_{\text{bulge}} \lesssim 10^{12.3} M_\odot$. More measurements in the range $M_{\text{bulge}} \sim 10^8 - 10^{10} M_\odot$ are needed to reveal whether intrinsic scatter in M_\bullet varies systematically across an extended range of bulge luminosities or masses.

The ϵ_0 term provides a reliable assessment of intrinsic scatter only if random measurement errors are small: measurements with large uncertainties can yield $\chi_\nu^2 \leq 1$ with no intrinsic scatter term. The root-mean-squared (RMS) residual between $\log(M_\bullet)$ and the global scaling relation is a more basic estimate, with no explicit dependence on measurement errors. Figure 5 shows that RMS closely follows ϵ_0 as a function of σ , L , and M_{bulge} . The qualitative agreement between the behavior of ϵ_0 and RMS indicates that variations in measurement errors are not responsible for the apparent trends in ϵ_0 .

5. SUMMARY AND DISCUSSION

We have compiled an updated sample of 72 black hole masses and host galaxy properties in Table A1; a more detailed version of Table A1 is available at <http://blackhole.berkeley.edu>. Compared with the 49 objects in G09, 25 black holes in our sample of 72 are new measurements and 18 masses are updates of previous values from improved data and/or modeling. Our present sample includes updated distances to 44 galaxies.

We presented revised fits for the $M_\bullet - \sigma$, $M_\bullet - L$, and $M_\bullet - M_{\text{bulge}}$ relations of our updated sample (Table 2 and Figures 1-3). Each relation is fit as a power-law: $\log_{10}(M_\bullet) = \alpha + \beta \log_{10}(X)$. Our best fit to the full sample of 72 galaxies with velocity dispersion measurements ($X \equiv \sigma/200 \text{ km s}^{-1}$) is $\alpha = 8.33 \pm 0.05$ and $\beta = 5.57 \pm 0.33$. A quadratic fit to the $M_\bullet - \sigma$ relation with an additional term $\beta_2 [\log_{10}(X)]^2$ gives $\beta_2 = 1.52 \pm 1.95$ and does not decrease the intrinsic scatter in M_\bullet . Including 92 additional upper limits for M_\bullet does not change the slope significantly: $\beta = 5.67 \pm 0.34$.

For the 44 early-type galaxies with reliable V-band luminosity measurements ($X \equiv L_V/10^{11} L_\odot$), we find $\alpha = 9.23 \pm 0.10$ and $\beta = 1.11 \pm 0.13$. For the 35 early-type galaxies with dynamical measurements of the bulge stellar mass ($X \equiv M_{\text{bulge}}/10^{11} M_\odot$), we find $\alpha = 8.46 \pm 0.08$ and $\beta = 1.05 \pm 0.11$.

We have also examined the black hole scaling relations for different subsamples of galaxies. When the galaxies are separated into early- and late-types and fit individually for the $M_\bullet - \sigma$ relation, we find nearly identical

slopes of $\beta = 5.08 \pm 0.38$ (early-types) and 5.06 ± 1.16 (late-types). The intercepts, however, differ significantly: $\alpha = 8.41 \pm 0.06$ for the early types, a factor of ~ 2 higher than $\alpha = 8.07 \pm 0.21$ for the late types. The steep global slope of 5.57 is therefore largely an effect of combining different galaxy types, each of which obey a shallower $M_\bullet - \sigma$ relation and different intercepts.

When the early-type galaxies are further divided into two subsamples based on their inner surface brightness profiles, the resulting $M_\bullet - \sigma$ relation has a significantly larger intercept for the core galaxies than the power-law galaxies (Table 2 and Figure 4a). The slopes of the $M_\bullet - L$ and $M_\bullet - M_{\text{bulge}}$ relations do not show statistically significant differences between core and power-law galaxies, but M_\bullet follows L and M_{bulge} more tightly in core galaxies than power-law galaxies (Table 2).

In the literature, the exact value of the $M_\bullet - \sigma$ slope has been much debated by observers and regarded as a key discriminator for models of the assembly and growth of supermassive black holes and their host galaxies by theorists. We suggest that the individual observed $M_\bullet - \sigma$ relations for the early- and late-type galaxies provide more meaningful constraints on theoretical models than the global relation. After all, these two types of galaxies are formed via different processes. Superficially, our measurement of $\beta = 5.57 \pm 0.33$ for the global $M_\bullet - \sigma$ relation favors thermally-driven wind models that predict $\beta \sim 5$ (e.g., Silk & Rees 1998) over momentum-driven wind models with $\beta \sim 4$ (e.g., Fabian 1999). For the subsamples, however, the early-type galaxies give $\beta > 4.0$ with 99.8% confidence ($\Delta\chi^2 = 7.9$ for $\epsilon_0 = 0.33$) and $\beta > 4.5$ with 93% confidence ($\Delta\chi^2 = 2.2$), whereas the late-type, core, and power-law galaxy subsamples are each consistent with $\beta = 4.5$ ($\Delta\chi^2 < 1$). The late-type and power-law samples cannot even exclude $\beta = 4.0$. Including central kinematics in the definition of σ further erodes the significance of high β for the early-type and core galaxy subsamples. More robust black hole measurements and more sophisticated theoretical models taking into account of galaxy types and environment (e.g. Zubovas & King 2012) are needed before stronger constraints can be obtained.

The intrinsic scatter in M_\bullet plotted in Figure 5 for different intervals of σ , L , and M_{bulge} serves as an independent test for theoretical models of the black hole and galaxy growths. Our dataset shows decreasing scatter in M_\bullet with increasing σ . However, there are currently insufficient data to probe the $30 - 100 \text{ km s}^{-1}$ range, where scatter in M_\bullet could identify the initial formation mechanism for massive black holes (Volonteri et al. 2008; Volonteri & Natarajan 2009). Theoretical models of hierarchical mergers in Λ CDM cosmology predict that scatter in M_\bullet should decline steadily with increasing stellar mass (M_\star), even when M_\bullet and M_\star are initially uncorrelated (Malbon et al. 2007; Peng 2007; Hirschmann et al. 2010; Jahnke & Macciò 2011). The semi-analytic models by Malbon et al. (2007), for instance, predict that black holes with present-day masses $> 10^8 M_\odot$ have gained most of their mass via black hole-black hole mergers, yielding extremely low scatter ($\epsilon_0 \sim 0.1$) at the upper end of the $M_\bullet - M_{\text{bulge}}$ relation. More recent models by Jahnke & Macciò (2011) use fully decoupled prescriptions for star formation and black hole growth, and attain a more realistic amount of scatter on average. Yet these

models still exhibit decreasing scatter as M_{bulge} increases from $\sim 10^9 M_{\odot}$ to $\sim 10^{11.5} M_{\odot}$. In comparison, we observe nearly constant scatter from $M_{\text{bulge}} \sim 10^{11} M_{\odot}$ to $10^{12} M_{\odot}$, beyond the highest bulge masses produced in the Jahnke & Macciò (2011) models.

Our final comment is that investigations using the $M_{\bullet}-\sigma$ correlation should consider the definition of σ , i.e., whether it is measured from an inner radius of zero or r_{inf} . We find that both definitions yield similar amounts of scatter in the $M_{\bullet}-\sigma$ relation (Table 2), so neither has a clear advantage for predicting M_{\bullet} . Excluding data within r_{inf} corresponds more closely to cases where r_{inf} is unresolved, such as seeing-limited galaxy surveys, high-redshift observations, or numerical simulations with limited spatial resolution. From a theoretical perspective, the evolutionary origin of an $M_{\bullet}-\sigma$ relation and the immediate effects of gravity may warrant separate consideration. On the other hand, the total gravitational potential of a galaxy includes its black hole. Our test of how redefining σ alters the $M_{\bullet}-\sigma$ relation has only considered nine galaxies for which data within r_{inf} contribute prominently to the spatially integrated velocity dispersion. At present, the full sample of M_{\bullet} and σ measurements comprises a heterogeneous selection of kinematic data. Rather than advocating a particular definition, we wish to call attention to the nuances of interpreting the $M_{\bullet}-\sigma$ relation and encourage future investigators to consider their options carefully.

Dynamical measurements of M_{\bullet} require substantial ob-

servational resources and careful analysis, and are often published individually. Nonetheless, recent and ongoing efforts are rapidly expanding the available M_{\bullet} measurements and revising the empirical black hole scaling relations. Our online database ⁴ is aimed to provide all researchers easy access to frequently updated compilation of supermassive black holes with direct dynamical mass measurements and their host galaxy properties. Updated scaling relations can be used to estimate M_{\bullet} more accurately in individual galaxies. This can improve our knowledge of Eddington rates and spectral energy distributions for accreting black holes, as well as time and distance scales for tidal disruption events. Moreover, the $M_{\bullet}-\sigma$ relation for quiescent black holes has been used to normalize the black hole masses obtained from reverberation mapping studies of active galaxies (Onken et al. 2004; Woo et al. 2010). This important calibration could be improved by addressing morphology biases in the reverberation mapping samples and the $M_{\bullet}-\sigma$ relations for different galaxy types.

This work is supported in part by NSF AST-1009663. NJM is supported by the Beatrice Watson Parrent Fellowship. We thank Karl Gebhardt, Tod Lauer, and John Blakeslee for useful discussions and Michael Reed for help with the data table and compilation. We thank the anonymous referee for constructive comments on our original manuscript.

⁴ <http://blackhole.berkeley.edu>

REFERENCES

- Atkinson, J. W., Collett, J. L., Marconi, A., et al. 2005, MNRAS, 359, 504
- Baes, M., Buyle, P., Hau, G. K. T., & Dejonghe, H. 2003, MNRAS, 341, L44
- Barth, A. J., Sarzi, M., Rix, H.-W., et al. 2001, ApJ, 555, 685
- Beifiori, A., Courteau, S., Corsini, E. M., & Zhu, Y. 2012, MNRAS, 419, 2497 (B12)
- Beifiori, A., Sarzi, M., Corsini, E. M., et al. 2009, ApJ, 692, 856
- Bender, R., Kormendy, J., Bower, G., et al. 2005, ApJ, 631, 280
- Bernardi, M., Hyde, J. B., Sheth, R. K., Miller, C. J., & Nichol, R. C. 2007, AJ, 133, 1741
- Blakeslee, J. P., Jordán, A., Mei, S., et al. 2009, ApJ, 694, 556
- Blakeslee, J. P., Cantiello, M., Mei, S., et al. 2010, ApJ, 724, 657
- Bogdán, Á., Forman, W. R., Kraft, R. P., et al. 2012, ApJ, 755, 25
- Bower, G. A., Green, R. F., Bender, R., et al. 2001, ApJ, 550, 75
- Boylan-Kolchin, M., Ma, C.-P., & Quataert, E. 2006, MNRAS, 369, 1081
- Braatz, J. A., Reid, M. J., Humphreys, E. M. L., et al. 2010, ApJ, 718, 657
- Burkert, A., & Tremaine, S. 2010, ApJ, 720, 516
- Cappellari, M., Neumayer, N., Reunanen, J., et al. 2009, MNRAS, 394, 660
- Cappellari, M., Verolme, E. K., van der Marel, R. P., et al. 2002, ApJ, 578, 787
- Cappellari, M., Bacon, R., Bureau, M., et al. 2006, MNRAS, 366, 1126
- Comroy, C., & van Dokkum, P. 2012, arXiv 1205.6473
- Cretton, N., & van den Bosch, F. C. 1999a, ApJ, 514, 704
- Dalla Bontà, E., Ferrarese, L., Corsini, E. M., et al. 2009, ApJ, 690, 537
- Davies, R. I., Thomas, J., Genzel, R., et al. 2006, ApJ, 646, 754
- de Francesco, G., Capetti, A., & Marconi, A. 2008, A&A, 479, 355
- Devereux, N., Ford, H., Tsvetanov, Z., & Jacoby, G. 2003, AJ, 125, 1226
- Emsellem, E., Dejonghe, H., & Bacon, R. 1999, MNRAS, 303, 495
- Faber, S. M., Tremaine, S., Ajhar, E. A., et al. 1997, AJ, 114, 1771
- Fabian, A. C. 1999, MNRAS, 308, L39
- Ferrarese, L. 2002, ApJ, 578, 90
- Ferrarese, L., & Ford, H. C. 1999, ApJ, 515, 583
- Ferrarese, L., Ford, H. C., & Jaffe, W. 1996, ApJ, 470, 444
- Ferrarese, L., & Merritt, D. 2000, ApJ, 539, L9
- Ferrarese, L., Côté, P., Jordán, A., et al. 2006, ApJS, 164, 334
- Gebhardt, K., Adams, J., Richstone, D., et al. 2011, ApJ, 729, 119
- Gebhardt, K., & Thomas, J. 2009, ApJ, 700, 1690
- Gebhardt, K., Bender, R., Bower, G., et al. 2000, ApJ, 539, L13
- Gebhardt, K., Richstone, D., Tremaine, S., et al. 2003, ApJ, 583, 92
- Gebhardt, K., Lauer, T. R., Pinkney, J., et al. 2007, ApJ, 671, 1321
- Ghez, A. M., Salim, S., Weinberg, N. N., et al. 2008, ApJ, 689, 1044
- Gillessen, S., Eisenhauer, F., Trippe, S., et al. 2009, ApJ, 692, 1075
- Glass, L., Ferrarese, L., Côté, P., et al. 2011, ApJ, 726, 31
- Graham, A. W. 2007, MNRAS, 379, 711
- . 2008, PASA, 25, 167
- . 2012, ApJ, 746, 113
- Graham, A. W., Colless, M. M., Busarello, G., Zaggia, S., & Longo, G. 1998, A&AS, 133, 325
- Graham, A. W., & Driver, S. P. 2007, ApJ, 655, 77
- Graham, A. W., Erwin, P., Caon, N., & Trujillo, I. 2001, ApJ, 563, L11
- Graham, A. W., Onken, C. A., Athanassoula, E., & Combes, F. 2011, MNRAS, 412, 2211
- Greene, J. E., Peng, C. Y., Kim, M., et al. 2010, ApJ, 721, 26
- Greenhill, L. J., Booth, R. S., Ellingsen, S. P., et al. 2003, ApJ, 590, 162
- Gültekin, K., Richstone, D. O., Gebhardt, K., et al. 2011, ApJ, 741, 38
- . 2009a, ApJ, 698, 198 (G09)
- . 2009b, ApJ, 695, 1577
- Häring, N., & Rix, H.-W. 2004, ApJ, 604, L89
- Harris, G. L. H., & Harris, W. E. 2011, MNRAS, 410, 2347
- Herrnstein, J. R., Moran, J. M., Greenhill, L. J., & Trotter, A. S. 2005, ApJ, 629, 719

- Hirschmann, M., Khochfar, S., Burkert, A., et al. 2010, *MNRAS*, 407, 1016
- Houghton, R. C. W., Magorrian, J., Sarzi, M., et al. 2006, *MNRAS*, 367, 2
- Hu, J. 2008, *MNRAS*, 386, 2242
- . 2009, arXiv 0908.2028
- Isobe, T., Feigelson, E. D., & Nelson, P. I. 1986, *ApJ*, 306, 490
- Jahnke, K., & Macciò, A. V. 2011, *ApJ*, 734, 92
- Jardel, J. R., Gebhardt, K., Shen, J., et al. 2011, *ApJ*, 739, 21
- Kelly, B. C. 2007, *ApJ*, 665, 1489
- Kondratko, P. T., Greenhill, L. J., & Moran, J. M. 2008, *ApJ*, 678, 87
- Kormendy, J., & Bender, R. 2009, *ApJ*, 691, L142
- . 2011, *Nature*, 469, 377
- Kormendy, J., Bender, R., & Cornell, M. E. 2011, *Nature*, 469, 374
- Kormendy, J., & Gebhardt, K. 2001, in *American Institute of Physics Conference Series*, Vol. 586, 20th Texas Symposium on relativistic astrophysics, ed. J. C. Wheeler & H. Martel, 363–381
- Kormendy, J., & Richstone, D. 1995, *ARA&A*, 33, 581
- Krajnović, D., McDermid, R. M., Cappellari, M., & Davies, R. L. 2009, *MNRAS*, 399, 1839
- Kuo, C. Y., Braatz, J. A., Condon, J. J., et al. 2011, *ApJ*, 727, 20
- Lauer, T. R., Tremaine, S., Richstone, D., & Faber, S. M. 2007c, *ApJ*, 670, 249
- Lauer, T. R., Faber, S. M., Richstone, D., et al. 2007a, *ApJ*, 662, 808
- Lauer, T. R., Gebhardt, K., Faber, S. M., et al. 2007b, *ApJ*, 664, 226
- Lavalley, M. P., Isobe, T., & Feigelson, E. D. 1992, in *Bulletin of the American Astronomical Society*, Vol. 24, *Bulletin of the American Astronomical Society*, 839–840
- Lodato, G., & Bertin, G. 2003, *A&A*, 398, 517
- Magorrian, J., Tremaine, S., Richstone, D., et al. 1998, *AJ*, 115, 2285
- Malbon, R. K., Baugh, C. M., Frenk, C. S., & Lacey, C. G. 2007, *MNRAS*, 382, 1394
- Marconi, A., & Hunt, L. K. 2003, *ApJ*, 589, L21
- McConnell, N. J., Ma, C.-P., Gebhardt, K., et al. 2011a, *Nature*, 480, 215
- McConnell, N. J., Ma, C.-P., Graham, J. R., et al. 2011b, *ApJ*, 728, 100
- McConnell, N. J., Ma, C.-P., Murphy, J. D., et al. 2012, *ApJ*, 756, 179
- McLure, R. J., & Dunlop, J. S. 2002, *MNRAS*, 331, 795
- . 2004, *MNRAS*, 352, 1390
- Merritt, D., & Ferrarese, L. 2001, *ApJ*, 547, 140
- Neumayer, N., Cappellari, M., Reunanen, J., et al. 2007, *ApJ*, 671, 1329
- Nowak, N., Saglia, R. P., Thomas, J., et al. 2008, *MNRAS*, 391, 1629
- Nowak, N., Saglia, R. P., Thomas, J., et al. 2007, *MNRAS*, 379, 909
- Nowak, N., Thomas, J., Erwin, P., et al. 2010, *MNRAS*, 403, 646
- Onken, C. A., Ferrarese, L., Merritt, D., et al. 2004, *ApJ*, 615, 645
- Park, D., Kelly, B. C., Woo, J.-H., & Treu, T. 2012, arXiv 1209.3773
- Peng, C. Y. 2007, *ApJ*, 671, 1098
- Pinkney, J., Gebhardt, K., Bender, R., et al. 2003, *ApJ*, 596, 903
- Pu, S. B., Saglia, R. P., Fabricius, M. H., et al. 2010, *A&A*, 516, A4
- Rusli, S. P. 2012, PhD thesis, Ludwig Maximilians Universität, München
- Rusli, S. P., Thomas, J., Erwin, P., et al. 2011, *MNRAS*, 410, 1223
- Sadoun, R., & Colin, J. 2012, arXiv 1204.0144
- Sani, E., Marconi, A., Hunt, L. K., & Risaliti, G. 2011, *MNRAS*, 413, 1479
- Sarzi, M., Rix, H.-W., Shields, J. C., et al. 2001, *ApJ*, 550, 65
- Schulze, A., & Gebhardt, K. 2011, *ApJ*, 729, 21
- Shen, J., & Gebhardt, K. 2010, *ApJ*, 711, 484
- Silk, J., & Rees, M. J. 1998, *A&A*, 331, L1
- Simien, F., & Prugniel, P. 2000, *A&AS*, 145, 263
- Spolaor, M., Forbes, D. A., Hau, G. K. T., Proctor, R. N., & Brough, S. 2008, *MNRAS*, 385, 667
- Tonry, J. L., Dressler, A., Blakeslee, J. P., et al. 2001, *ApJ*, 546, 681
- Tremaine, S., Gebhardt, K., Bender, R., et al. 2002, *ApJ*, 574, 740
- van den Bosch, R. C. E., & de Zeeuw, P. T. 2010, *MNRAS*, 401, 1770
- van der Marel, R. P., & van den Bosch, F. C. 1998, *AJ*, 116, 2220
- Verolme, E. K., Cappellari, M., Copin, Y., et al. 2002, *MNRAS*, 335, 517
- Vilardell, F., Jordi, C., & Ribas, I. 2007, *A&A*, 473, 847
- Volonteri, M., Lodato, G., & Natarajan, P. 2008, *MNRAS*, 383, 1079
- Volonteri, M., & Natarajan, P. 2009, *MNRAS*, 400, 1911
- Volonteri, M., Natarajan, P., & Gültekin, K. 2011, *ApJ*, 737, 50
- Walsh, J. L., Barth, A. J., & Sarzi, M. 2010, *ApJ*, 721, 762
- Walsh, J. L., van den Bosch, R. C. E., Barth, A. J., & Sarzi, M. 2012, *ApJ*, 753, 79
- Williams, M. J., Bureau, M., & Cappellari, M. 2010, *MNRAS*, 409, 1330
- Wold, M., Lacy, M., Käufel, H. U., & Siebenmorgen, R. 2006, *A&A*, 460, 449
- Woo, J.-H., Treu, T., Barth, A. J., et al. 2010, *ApJ*, 716, 269
- Wyithe, J. S. B. 2006a, *MNRAS*, 365, 1082
- . 2006b, *MNRAS*, 371, 1536
- Zasov, A. V., Petrochenko, L. N., & Cherepashchuk, A. M. 2005, *Astronomy Reports*, 49, 362
- Zubovas, K., & King, A. R. 2012, *MNRAS*, 426, 2751

TABLE A1
GALAXIES WITH DYNAMICAL MEASUREMENTS OF M_{\bullet}

Galaxy	M_{\bullet} (+, -) (M_{\odot})	Ref.	σ (km s^{-1})	$\log L_V$	M_{bulge} (M_{\odot})	Ref.	r_{inf} (arcsec)	Morph.	D (Mpc)	Method
Milky Way ^a	4.1 (0.6,0.6) e6	1,2	103 ± 20				43	S	0.008	stars
A1836-BCG	3.9 (0.4,0.6) e9	3	288 ± 14	11.26 ± 0.06			0.27	E (C)	157.5	gas
A3565-BCG	1.4 (0.3,0.2) e9	3	322 ± 16	11.24 ± 0.06			0.22	E (C)	54.4	gas
Circinus	1.7 (0.4,0.3) e6	4	158 ± 18				0.02	S	4.0	masers
IC 1459	2.8 (1.1,1.2) e9	5	315 ± 16	10.96 ± 0.06	3.07e11	45	0.81	E (C)	30.9	stars
N221 (M32) ^y	2.6 (0.5,0.5) e6	6	75 ± 3	8.52 ± 0.02	7.62e8	45	0.57	E (I)	0.73	stars
N224 (M31) ^y	1.4 (0.8,0.3) e8	7	160 ± 8				6.5	S	0.73	stars
N524 ^w	8.6 (1.0,0.4) e8	8	235 ± 12	10.62 ± 0.04			0.57	S0 (C)	24.2	stars
N821 ^w	1.7 (0.7,0.7) e8	9	209 ± 10	10.36 ± 0.05	1.92e11	9	0.14	E (I)	23.4	stars
N1023 ^w	4.0 (0.4,0.4) e7	10	205 ± 10	10.06 ± 0.11	6.49e10	45	0.08	S0 (pl)	10.5	stars
N1194 ^b	6.8 (0.3,0.3) e7	11	148 ⁺²⁶ ₋₂₂				0.05	S0	55.5	masers
N1300	7.1 (3.4,1.8) e7	12	218 ± 10				0.07	S	20.1	gas
N1316 ^x	1.7 (0.3,0.3) e8	13	226 ± 11	11.18 ± 0.05			0.14	E (I)	21.0	stars
N1332 ^w	1.5 (0.2,0.2) e9	14	328 ± 16	10.16 ± 0.05			0.54	S0 (pl)	22.7	stars
N1374 ^x	5.9 (0.6,0.5) e8	15	146 ± 7	10.10 ± 0.05	5.79e10	15	1.3	E (C)	19.6	stars
N1399 ^{c,x}	5.1 (0.6,0.7) e8	16	296 ± 15	10.78 ± 0.04	3.98e11	46	0.25	E (C)	20.9	stars
N1399 ^{c,x}	1.3 (0.5,0.7) e9	17	296 ± 15	10.78 ± 0.04	3.98e11	46	0.63	E (C)	20.9	stars
N1407 ^w	4.7 (0.7,0.5) e9	15	274 ± 14	11.05 ± 0.05	1.00e12	15	1.9	E (C)	29.0	stars
N1550	3.9 (0.7,0.7) e9	15	289 ± 14	10.87 ± 0.05			0.78	E (I)	53.0	stars
N2273 ^b	7.8 (0.4,0.4) e6	11	144 ⁺¹⁸ ₋₁₅				0.01	S	26.8	masers
N2549 ^w	1.4 (0.1,0.4) e7	8	145 ± 7	9.55 ± 0.04	1.99e10	8	0.05	S0 (pl)	12.7	stars
N2787 ^w	4.1 (0.4,0.5) e7	18	189 ± 9				0.14	S0 (pl)	7.5	gas
N2960 ^b	1.21 (0.05,0.05) e7	11	166 ⁺¹⁶ ₋₁₅				0.01	S	75.3	masers
N3031 (M81)	8.0 (2.0,1.1) e7	19	143 ± 7				0.85	S	4.1	gas
N3091	3.7 (0.1,0.5) e9	15	307 ± 15	11.00 ± 0.05			0.66	E (C)	52.7	stars
N3115 ^w	8.9 (5.1,2.7) e8	20	230 ± 11	10.34 ± 0.02	1.57e11	45	1.6	S0 (pl)	9.5	stars
N3227	1.5 (0.5,0.8) e7	21	133 ± 12				0.04	S	17.0	stars
N3245 ^w	2.1 (0.5,0.6) e8	22	205 ± 10		7.00e10	45	0.21	S0 (pl)	21.5	gas
N3368 ^w	7.6 (1.6,1.5) e6	23	122 ⁺²⁸ ₋₂₄				0.04	S	10.6	stars
N3377 ^w	1.8 (0.9,0.9) e8	9	145 ± 7	9.93 ± 0.04	2.35e10	9	0.69	E (pl)	11.0	stars
N3379 (M105) ^w	4.2 (1.0,1.1) e8	24	206 ± 10	10.29 ± 0.01	6.86e10	45	0.83	E (C)	10.7	stars
N3384 ^w	1.1 (0.5,0.5) e7	9	143 ± 7	9.89 ± 0.09	1.90e10	9	0.04	S0 (pl)	11.5	stars
N3393	3.3 (0.2,0.2) e7	25	148 ± 10				0.03	S	53.6	masers
N3489 ^w	6.0 (0.8,0.9) e6	23	100 ⁺¹⁵ ₋₁₁				0.04	S0	12.0	stars
N3585 ^w	3.3 (1.5,0.6) e8	26	213 ± 10	10.66 ± 0.08	1.60e11	26	0.31	S0 (I)	20.6	stars
N3607 ^{d,w}	1.4 (0.4,0.5) e8	26	229 ± 11				0.10	E (C)	22.6	stars
N3608 ^w	4.7 (1.0,1.0) e8	9	182 ± 9	10.34 ± 0.04	7.66e10	9	0.55	E (C)	22.8	stars
N3842	9.7 (3.0,2.5) e9	27	270 ± 14	11.20 ± 0.05	1.55e12	44	1.2	E (C)	98.4	stars
N3998 ^w	8.5 (0.7,0.7) e8	28	272 ± 14	9.91 ± 0.04			0.71	S0 (pl)	14.3	stars
N4026 ^w	1.8 (0.6,0.3) e8	26	180 ± 9	9.73 ± 0.08	2.81e10	26	0.37	S0 (pl)	13.4	stars
N4258 ^w	3.67 (0.01,0.01) e7	29	115 ± 10				0.35	S	7.0	masers
N4261 ^w	5.3 (1.1,1.1) e8	30	315 ± 15	11.00 ± 0.02	8.26e11	45	0.15	E (C)	32.6	gas
N4291 ^w	9.8 (3.1,3.1) e8	9	242 ± 12	10.25 ± 0.05	9.96e10	9	0.56	E (C)	26.6	stars
N4342 ^z	4.6 (2.6,1.5) e8	31	225 ± 11		1.80e10	45	0.35	S0 (pl)	23.0	stars
N4374 (M84) ^x	9.2 (1.0,0.8) e8	32	296 ± 14	10.98 ± 0.02	3.62e11	45	0.51	E (C)	18.5	gas
N4388 ^b	8.8 (0.2,0.2) e6	11	107 ⁺⁸ ₋₇				0.03	S	19.8	masers
N4459 ^x	7.0 (1.3,1.4) e7	18	167 ± 8	10.31 ± 0.02			0.14	E (pl)	16.0	gas
N4472 (M49) ^x	2.5 (0.6,0.1) e9	15	300 ± 15	11.05 ± 0.05	8.98e11	15	1.3	E (C)	16.7	stars
N4473 ^x	8.9 (4.5,4.4) e7	9	190 ± 9	10.29 ± 0.02	1.61e11	9	0.15	E (C)	15.2	stars
N4486 (M87) ^x	6.2 (0.3,0.4) e9	33	324 ⁺²⁸ ₋₁₆	11.08 ± 0.02	1.31e12	47	3.1	E (C)	16.7	stars
N4486A ^x	1.4 (0.5,0.5) e7	34	111 ± 5	9.48 ± 0.02			0.06	E (pl)	18.4	stars
N4564 ^{e,x}	8.8 (2.4,2.4) e7	9	162 ± 8		4.66e10	45	0.19	S0 (pl)	15.9	stars
N4594 (M104) ^w	6.7 (0.5,0.4) e8	35	230 ± 12			45	1.1	S	10.0	stars
N4596	8.4 (3.6,2.5) e7	18	136 ± 6				0.22	S0 (pl)	18.0	gas
N4649 (M60) ^x	4.7 (1.1,1.0) e9	36	341 ± 17	10.99 ± 0.02	7.72e11	36	2.2	E (C)	16.5	stars
N4697 ^x	2.0 (0.2,0.2) e8	9	177 ± 8	10.46 ± 0.04	1.29e11	9	0.46	E (pl)	12.5	stars
N4736 (M94) ^{f,w}	6.8 (1.6,1.6) e6	37	112 ± 6				0.10	S	5.0	stars
N4826 (M64) ^{f,w}	1.6 (0.4,0.4) e6	37	96 ± 5				0.02	S	7.3	stars
N4889	2.1 (1.6,1.55) e10	27	347 ± 17	11.48 ± 0.05	1.75e12	46	1.5	E (C)	103.2	stars

Table A1, continued

Galaxy	M_{\bullet} (+, -) (M_{\odot})	Ref.	σ (km s^{-1})	$\log L_V$	M_{bulge} (M_{\odot})	Ref.	r_{inf} (arcsec)	Morph.	D (Mpc)	Method
N5077	8.0 (5.0,3.3) e8	38	222 ± 11	10.75 ± 0.05	3.66e11	38	0.32	E (C)	44.9	gas
N5128 (Cen A) ^{g,w}	5.9 (1.1,1.0) e7	39	150 ± 7	10.60 ± 0.03			0.60	S0/E (C)	4.1	stars
N5516	4.0 (0.1,1.1) e9	15	306 ± 26	11.22 ± 0.05			0.63	E (C)	60.1	stars
N5576 ^w	1.7 (0.3,0.4) e8	26	183 ± 9	10.39 ± 0.05	9.58e10	26	0.18	E (C)	25.7	stars
N5845 ^w	4.9 (1.5,1.6) e8	9	234 ± 11	9.75 ± 0.05	3.36e10	9	0.31	E (pl)	25.9	stars
N6086	3.8 (1.7,1.2) e9	40	318 ± 16	11.23 ± 0.05	1.43e12	40	0.24	E (C)	139.1	stars
N6251	6.0 (2.0,2.0) e8	41	290 ± 14		5.60e11	46	0.06	E (pl)	106.0	gas
N6264 ^b	3.03 (0.05,0.04) e7	11	158_{-14}^{+16}				0.01	S	145.4	masers
N6323 ^b	9.8 (0.1,0.1) e6	11	158_{-23}^{+28}				0.003	S	110.5	masers
N7052	4.0 (2.8,1.6) e8	42	266 ± 13	10.92 ± 0.04	3.50e11	45	0.07	E (C)	70.9	gas
N7582	5.5 (1.6,1.1) e7	43	156 ± 19				0.09	S	22.3	gas
N7619 ^w	2.3 (1.2,0.1) e9	15	313 ± 16	11.07 ± 0.05			0.39	E (C)	53.9	stars
N7768	1.3 (0.5,0.4) e9	44	257 ± 13	11.09 ± 0.05	1.16e12	44	0.14	E (C)	112.8	stars
U3789 ^b	1.08 (0.06,0.05) e7	11	107_{-12}^{+13}				0.02	S	48.4	masers

Notes: The first reference column corresponds to the black hole mass measurement, and the second corresponds to the measurement of M_{\star}/L used to compute M_{bulge} . Bulge luminosity L_V is in solar units. Quoted errors (+, -) for M_{\bullet} are 68% confidence intervals. We assume 0.24 dex uncertainty for all M_{bulge} values. Morphologies include designations for power-law (pl), core (C), and intermediate (I) surface brightness profiles.

References: (1 = Ghez et al. 2008) ; (2 = Gillessen et al. 2009) ; (3 = Dalla Bontà et al. 2009) ; (4 = Greenhill et al. 2003) ; (5 = Cappellari et al. 2002) ; (6 = Verolme et al. 2002) ; (7 = Bender et al. 2005) ; (8 = Krajnović et al. 2009) ; (9 = Schulze & Gebhardt 2011) ; (10 = Bower et al. 2001) ; (11 = Kuo et al. 2011) ; (12 = Atkinson et al. 2005) ; (13 = Nowak et al. 2008) ; (14 = Rusli et al. 2011) ; (15 = Rusli 2012) ; (16 = Gebhardt et al. 2007) ; (17 = Houghton et al. 2006) ; (18 = Sarzi et al. 2001) ; (19 = Devereux et al. 2003) ; (20 = Emsellem et al. 1999) ; (21 = Davies et al. 2006) ; (22 = Barth et al. 2001) ; (23 = Nowak et al. 2010) ; (24 = van den Bosch & de Zeeuw 2010) ; (25 = Kondratko et al. 2008) ; (26 = Gültekin et al. 2009b) ; (27 = McConnell et al. 2011a) ; (28 = Walsh et al. 2012) ; (29 = Herrnstein et al. 2005) ; (30 = Ferrarese et al. 1996) ; (31 = Cretton & van den Bosch 1999a) ; (32 = Walsh et al. 2010) ; (33 = Gebhardt et al. 2011) ; (34 = Nowak et al. 2007) ; (35 = Jardel et al. 2011) ; (36 = Shen & Gebhardt 2010) ; (37 = Kormendy et al. 2011) ; (38 = de Francesco et al. 2008) ; (39 = Cappellari et al. 2009) ; (40 = McConnell et al. 2011b) ; (41 = Ferrarese & Ford 1999) ; (42 = van der Marel & van den Bosch 1998) ; (43 = Wold et al. 2006) ; (44 = McConnell et al. 2012) ; (45 = Häring & Rix 2004) ; (46 = Magorrian et al. 1998) ; (47 = Gebhardt & Thomas 2009).

Notes on individual galaxies:

^a The literature contains a large number of estimates for the velocity dispersion of our Galaxy's bulge, using different kinematic tracers at different radii. We use the radially averaged measurement of $\sigma = 103 \pm 20 \text{ km s}^{-1}$ from Tremaine et al. (2002).

^b Maser-based black hole masses for several galaxies are presented in Greene et al. (2010) and Kuo et al. (2011). We use the velocity dispersions presented in Greene et al. (2010). For consistency with the rest of our sample, we use the black hole masses from Kuo et al. (2011), which agree with the values in Greene et al. (2010) but do not include distance uncertainties in the overall uncertainty for M_{\bullet} . Braatz et al. (2010) provide an updated distance and black hole mass for UGC 3789, which are consistent with the values we adopt from Kuo et al. (2011).

^c Following G09, our sample includes two distinct measurements for NGC 1399. We weight each of these measurements by 50% when performing fits to the black hole scaling relations.

^d The literature contains two inconsistent estimates of the V -band luminosity of NGC 3607: $M_V = -21.62$ in G09, and $M_V = -19.88$ in Lauer et al. (2007a).

^e The literature contains two inconsistent estimates of the V -band bulge luminosity of NGC 4564: $M_V = -19.60$ in G09, and $M_V = -20.26$ in Lauer et al. (2007a).

^f Bulge luminosities for NGC 4736 and NGC 4826 were included in the sample of McConnell et al. (2011a) and their fit to the $M_{\bullet} - L$ relation. These luminosities corresponded to pseudobulges identified in Kormendy et al. (2011), and we have not included them in our present fits.

^g The stellar dynamical measurement of M_{\bullet} in NGC 5128 by Cappellari et al. (2009) is fully consistent with the molecular gas measurement $M_{\bullet} = 5.3_{-0.4}^{+0.6} M_{\odot}$ by Neumayer et al. (2007).

^w We have updated the distances to 29 galaxies using surface brightness fluctuation measurements from Tonry et al. (2001), with the corrections suggested by Blakeslee et al. (2010).

^x We have updated the distances to 12 galaxies using surface brightness fluctuation measurements from Blakeslee et al. (2009), which are based on data from ACS on the *Hubble Space Telescope*.

^y We have adopted a distance of 0.73 Mpc to M31, based on Cepheid variable measurements by Vilardell et al. (2007). We assume that M31 and M32 lie at the same distance.

^z For NGC 4342, we have adopted the distance of 23 Mpc by Bogdán et al. (2012).